

Do Planetary Encounters Reset Surfaces of Near Earth Asteroids?

David Nesvorný¹, William F. Bottke¹, David Vokrouhlický², Clark R. Chapman¹

and

Scot Rafkin¹

(1) *Department of Space Studies, Southwest Research Institute, 1050 Walnut St., Suite 300, Boulder, Colorado 80302, USA*

(2) *Institute of Astronomy, Charles University, V Holešovičkách 2, 180 00 Prague 8, Czech Republic*

ABSTRACT

Processes such as the solar wind sputtering and micrometeorite impacts can modify optical properties of surfaces of airless bodies. This explains why spectra of the main belt asteroids, exposed to these ‘space weathering’ processes over eons, do not match the laboratory spectra of ordinary chondrite (OC) meteorites. In contrast, an important fraction of Near Earth Asteroids (NEAs), defined as Q-types in the asteroid taxonomy, display spectral attributes that are a good match to OCs. Here we study the possibility that the Q-type NEAs underwent recent encounters with the terrestrial planets and that the tidal gravity (or other effects) during these encounters exposed fresh OC material on the surface (thus giving it the Q-type spectral properties). We used numerical integrations to determine the statistics of encounters of NEAs to planets. The results were used to calculate the fraction and orbital distribution of Q-type asteroids expected in the model as a function of the space weathering timescale, t_{sw} (see main text for definition), and maximum distance, r^* , at which planetary encounters can reset the surface. We found that $t_{\text{sw}} \sim 10^6$ yr (at 1 AU) and $r^* \sim 5 R_{\text{pl}}$, where R_{pl} is the planetary radius, best fit the data. Values $t_{\text{sw}} < 10^5$ yr would require that $r^* > 20 R_{\text{pl}}$, which is probably implausible because these very distant encounters should be irrelevant. Also, the fraction of Q-type NEAs would be probably much larger than the one observed if $t_{\text{sw}} > 10^7$ yr. We found that $t_{\text{sw}} \propto q^2$, where q is the perihelion distance, expected if the solar wind sputtering controls t_{sw} , provides a better match to the orbital distribution of Q-type NEAs than models with fixed t_{sw} . We also discuss how the Earth magnetosphere and radiation effects such as YORP can influence the spectral properties of NEAs.

Subject headings: Near-Earth Objects; Asteroids, surfaces; Asteroids, dynamics;
Infrared observations; Meteorites

1. Introduction

Measurements of the spectral properties of Near Earth Asteroids (NEAs) provide important evidence concerning the relationship between asteroids and the most common class of meteorites known as the ordinary chondrites (OCs). The tendency toward seeing OC-like spectral attributes among NEAs has been noted in multi-filter color observations (Rabinowitz 1998, Whiteley 2001), and in visible and near-infrared spectrophotometric surveys (Binzel et al. 1996, 2004, 2010). In contrast, no spectral analogs of OCs have been found to date among the ~ 2000 surveyed main belt asteroids (MBAs), except for a case related to identified recent asteroid collisions (Mothé-Diniz and Nesvorný 2008).

The lack of spectrophotometric analogs for OC meteorites in the main belt is a long-debated and fundamental problem. It is now generally accepted that processes similar to those acting on the Moon, such as solar wind sputtering and micrometeorite impacts (Gold 1955, Pieters et al. 2000, see Hapke 2001 and Chapman 2004 for reviews), can darken and redden the initially OC-like spectrum of a fresh asteroid surface, giving it the ‘weathered’ appearance (see Chapman 1996 and Clark et al. 2001, 2002a,b for direct evidence for asteroid space weathering processes from the NEAR-Shoemaker and Galileo spacecrafts). In the following text we will refer to processes that alter optical properties of surfaces of airless bodies as the ‘space weathering’ (SW) effects.

Since the SW processes should affect the MBAs and NEAs in roughly the same way (see, e.g., Marchi et al. 2006 for a study of the SW dependence on heliocentric distance), it may seem puzzling why a significant fraction of NEAs has an unweathered appearance (Binzel et al. 2004) while practically all spectroscopically surveyed MBAs are weathered. Several explanations have been proposed.

To simplify the discussion of different models described below, we will use the following terminology taken from the standard asteroid taxonomy (Bus and Binzel 2002, DeMeo et

al. 2009). We will define three categories of asteroid spectra: (1) Q-type spectra with deep absorption bands and shallow spectral slope similar to that of most OC meteorites in the RELAB database¹; (2) S-type spectra with shallow absorption bands and relatively steep spectral slope similar to that of weathered OCs; and (3) Sq-type spectra as the intermediate case between S and Q. See Bus and Binzel (2002) and DeMeo et al. (2009) for a formal definition of these categories. We will assume that asteroids with the Q-type spectra have essentially unweathered surfaces with OC-like mineralogy; the Sq- and S-type asteroids will be assumed to have moderately and strongly weathered surfaces with OC-like mineralogy.

About 20% of chondritic NEAs surveyed at visible and/or near-infrared wavelengths have Q-type spectra while this fraction is essentially zero among MBAs. The standard interpretation of these results has been based on the presumption that Q-type asteroids are likely to be small. Indeed, the current spectrophotometric surveys of MBAs are largely incomplete in the size range of typical NEAs with diameters less than a few km. Special emphasis has therefore been given to asteroid-size-dependent processes, such as immaturity of regoliths on small asteroids and/or the shorter collisional lifetime of smaller asteroids (e.g., Johnson and Fanale 1973, Binzel et al. 1996, 2004, Rabinowitz 1998, Whiteley 2001).

One possibility is that the observed spectral variations may be related to particle-size effects (Johnson and Fanale 1973), where the decreasing gravity results in a different size distribution of surface particles on typically smaller NEAs than on larger MBAs. However, the photometric parameters indicative of particle-size effects show little evidence of an asteroid diameter dependence, thereby giving doubt to this explanation (e.g., Clark et al. 2001, Masiero et al. 2009).

Binzel et al. (2004) hypothesized that the SW size-dependency was because the survival lifetime against catastrophic disruption decreases with decreasing size. Thus, on average, as we examine smaller and smaller objects, we should see younger and younger surfaces. Surfaces showing Q-type spectral properties should thus exist, on average, only among the smallest asteroids, which become easy spectroscopic targets only when they enter into NEA space. Large, OC-like asteroids in the main belt should have, on average, space-weathered spectral properties, explaining why they are taxonomically classified as S types.

¹<http://www.planetary.brown.edu/relab/>

2. NJWI05 Model

Nesvorný et al. (2005; hereafter NJWI05) pointed out several problems with this “standard model”. For example, the estimates of SW rates (Chapman et al. 2007, Mothé-Diniz and Nesvorný 2008, Vernazza et al. 2009) suggest that SW probably operates on timescales <10 My (or perhaps even $\lesssim 1$ My) to change an initially fresh Q-type surface into one that is partially weathered (corresponding to Sq). The SW process then probably continues to approach full maturity only after Gys of evolution (Jedicke et al. 2004, NJWI05, Willman et al. 2008). If so, the standard model would imply that the observed Q-type NEAs should have surface ages that are <10 My.

This implication of the standard scenario is at odds with the collisional and dynamical models of the NEAs’ origin because it would imply that $\sim 20\%$ of chondritic NEAs were produced by collisional breakups of large bodies within the past <10 My. In contrast, models predict much longer durations for processes like the Yarkovsky effect and weak resonances to insert km-sized MBAs into the planet-crossing space (e.g., Migliorini et al. 1998, Bottke et al. 2002, Morbidelli and Vokrouhlický 2003), and collisional lifetimes >100 My (e.g., Bottke et al. 2005). Whiteley (2001) discussed additional objections to the standard model.

More recently, as a test of the standard model, P. Vernazza and Mothé-Diniz et al. (2009) conducted a spectroscopic survey of ≈ 100 diameter $D \lesssim 5$ km asteroids in the inner main belt. With only one possible (but uncertain) Q-type candidate detected (Mothé-Diniz et al. 2009), this survey indicates that the Q-type asteroids are rare even among small MBAs. This rules out the standard scenario that attempts to explain spectrophotometric differences between NEAs and MBAs as chiefly due to size-dependent effects.

To resolve these problems, NJWI05 proposed a new model for the origin of Q-type NEAs by postulating that the optically-active layer on their surface has been recently reset by the *effects of tidal gravity during encounters of these bodies to the terrestrial planets*. For example, applied tidal stresses applied may cause elements of a fractured body to move with respect to each other, ballistically displace surface material, or even liberate the surface layers from the asteroid. Alternatively, if the tidal torque spins up an asteroid, the weathered regolith layers can be removed by carrying away the excess angular momentum.

To show the plausibility of this idea, NJWI05 estimated that a typical NEA suffers on

average about one encounter to within 2 Roche radii (R_{Roche}) from the Earth every ≈ 5 My. This time interval between encounters is comparable with the average orbital lifetime of NEAs (≈ 5 My according to Bottke et al. 2002) and is also comparable with the range of the SW timescale discussed above. Consequently, if tidal encounters at $2R_{\text{Roche}}$ can reset surfaces, Q-type NEAs should be numerous. For comparison, encounters up to five planetary radii (this limit depends on the NEA’s shape and spin vector) can produce strong shape distortions of a rubble-pile NEA and material stripping up to 10% of the NEA’s pre-encounter mass (Richardson et al. 1998).

Strong evidence supporting the NJWI05 model comes from the observed orbital distribution of Q-type NEAs. Several trends were pointed out (Nesvorný et al. 2004, NJWI05, Marchi et al. 2006): (a) the proportion of Q-type NEAs increases with decreasing perihelion distance q ; (b) the orbital distribution of known Q-type NEAs has a sharp edge at $q \sim 1$ AU; and (c) concentrations of Q-type NEAs occur for values of q that correspond to large collision probability with the terrestrial planets ($q = 1.0$ and 0.72 AU for Earth and Venus; see, e.g., Morbidelli and Gladman 1998). This correlation of the orbital distribution of Q-type NEAs with the collision probability is expected in the NJWI05 model because orbits with large collision probability also have frequent close encounters with the terrestrial planets (e.g., Bottke & Melosh 1996). Thus, the surfaces of these objects are expected to be ‘fresher’ on average showing fewer signs of the SW effects.

Recently, Binzel et al. (2010; hereafter B10) presented results supporting the NJWI05 model. They used a taxonomic classification based on the near-infrared (near-IR) spectroscopy which should more closely characterize surface mineralogy than previous taxonomies based on the visible wavelengths. We have verified, however, that there exists a very good correlation between the visible and near-IR classification of Q types. For example, from 6 NEAs that were classified as Qs from the visible spectra before IR data became available, 5 were classified as Qs based on the near-IR spectra and only 1 must have been re-classified as Sq. This shows that the use of the near-IR data does not really change the problem.

B10 numerically integrated the orbits of 95 selected asteroids (Q-, Sq-, and S-type NEAs and more distant Mars-crossers) for 0.5 My, recorded the history of their close encounters to the Earth and statistically analyzed the encounters in an attempt to correlate the statistics with spectroscopic type. Two main results were obtained in B10:

(1) 20 Q- and 55 S/Sq-type NEAs can collide with the Earth in 0.5 My (although the actual probability of such a collision is low). Conversely, none of the remaining 13 NEAs and 7 Mars-crossing asteroids (MCAs) included in the study, all S and Sq, have any chance of impact in 0.5 My. The time interval of 0.5 My used in the B10 study was motivated by the recent estimate of the SW timescale in Vernazza et al. (2009) where it was proposed, based on a comparative study of asteroid families and OC meteorites, that SW acts on <1 My to fully alter an asteroid spectrum from Q to S. Adopting this timescale, B10 computed that the probability that *all* known Q-types would fall into the former category by chance (asteroids with a possible impact) is only $(75/95)^{20} \approx 0.9\%$. Thus, they concluded, the lack of Qs in the latter group is unlikely to happen by chance.

The B10 study therefore showed that the Mars-crossing asteroids and distant NEAs on orbits decoupled from the Earth (i.e., those that have large q and no Earth encounters at all) are not Qs. This trend has already been noted before (Nesvorný et al. 2004, 2005, Marchi et al. 2006). The statistical significance assigned to the results by B10 sensitively depends on the selected sample. For example, the significance of ‘not finding Qs among 20 distant NEAs and Mars-crossers’ would drop to only about 2σ if Mars-crossers were excluded from the analysis, as they should because they are not NEAs. If, on the other hand, all non-NEAs were included in the analysis, the result becomes obvious because there are no known Q-type asteroids in the main belt (except those in the young families). We discuss this issue in more detail in §3.

(2) B10 used the observed fraction of Q-type NEAs to estimate that encounters up to 16 Earth radii (i.e., $\approx 5 R_{\text{Roche}}$) should give the asteroid surface a Q-type appearance. This is at odds with our understanding of the effects of tidal gravity because it would be surprising if these very distant encounters could lead to any displacement of the surface regolith (e.g., Richardson et al. 1998, Walsh and Richardson 2008).

This problem could indicate that some of the assumptions used in B10 may be invalid. For example, studies of asteroid families, lunar craters and some laboratory experiments suggest that the SW timescale, or at least the late stage of SW when the regolith gardening processes presumably become important, can last $\gg 1$ My (e.g., Pieters et al. 2000, Sasaki et al. 2001, Jedicke et al. 2004, NJWI05, Willman et al. 2008). On the other hand, experiments with the He ion bombardment of olivine powders conducted in Loeffler et al.

(2009) suggest the SW timescale $\ll 1$ My at 1 AU. The specific choice of the SW timescale in B10 is therefore not very well justified.

Here we study encounters of NEAs to the terrestrial planets and show that the B10’s analysis was incomplete. It turns out to be important, as originally proposed by NJWI05, to account not only for the encounters of NEAs to Earth but also to Venus. Once Venus encounters are included (see §3), the required encounter distance drops from 16 to ≈ 10 planetary radii (i.e., by a factor of $(16/10)^3 \approx 4$ in the strength of tidal perturbation). In addition, we find that the critical distance of planetary encounters, r^* , sensitively depends on the the assumed SW timescale. When the later is set to 1 My, for example, $r^* \approx 5\text{--}7$ planetary radii, which is a much more reasonable value than the B10 estimate.

The method used in B10 (see following §3) has its limitations because it is difficult, even in the statistical sense, to reconstruct the history of past planetary encounters by numerical integrations of present orbits into the past. To circumvent this problem, in §4 we develop a NEA model by forward orbital integrations of asteroids from their sources in the asteroid belt. This method is similar to that used by Bottke et al. (2002) only this time we focus on the statistics of encounters of NEAs to the terrestrial planets. The NEA model allows us to consider a wide range of SW timescales, including the long ones that cannot be studied by backward integrations of orbits.

3. Analysis of Planetary Encounters

We selected 95 NEAs and Mars-crossing asteroids (MCAs) with known Q, Sq or S taxonomic classification from the near-IR taxonomic catalog (DeMeo et al. 2009; Fig. 1). This selection is identical to that in B10; see Table 1 in Supplementary Material of B10 for the complete list. Starting from the current epoch we numerically integrated the orbits of the selected objects into the past and recorded all planetary encounters in 1 My (longer timescale is considered in section 4). This encounter record needs to be analyzed statistically because the integrated orbits are strongly chaotic.

In addition to the nominal orbit of each object we also followed 100 orbital clones. The clones were normally distributed within the appropriate orbit-determination uncertainty

limits around the nominal orbit (both taken from NEODyS²). In addition to gravitational perturbations from 8 planets (Mercury to Neptune), the orbits were also subject to the Yarkovsky force whose strength was chosen to sample the full range appropriate for each NEA’s size (Bottke et al. 2006). We used the Swift integrator (Levison and Duncan 1994) and 1 day time step. We found that shorter time steps produce results that are statistically equivalent to those obtained with the 1 day step.

By analyzing planetary encounters recorded in our integrations we found that the encounters with Venus are as important as those with the Earth. To show this, we normalized the distance of encounters to each planet by the planetary radius, R_{pl} , which is roughly an appropriate scaling for tidal gravity (e.g., Richardson et al. 1998), and calculated the minimal encounter distance, $R_{\text{min}}(t)$, reached in time t . This calculation was done for all clones of each individual object. We then determined the median \bar{R}_{min} over clones. The median minimum distance has the following statistical meaning: a NEA with given $\bar{R}_{\text{min}}(t) = r$ has a 50% chance to have close encounter at less than r planetary radii from a planet in time t . For illustration, Fig. 2 shows the distribution of encounters for $t = 0.5$ My and $\bar{R}_{\text{min}}(t)$ for asteroid 1862 Apollo. Note, for example, that $\bar{R}_{\text{min}}(t = 0.5\text{My})$ for the encounters of 1862 Apollo to Venus and Earth are 9.5 and 20.3 R_{pl} , respectively, while it is only 8 R_{pl} when all planetary encounters are combined.

In the next step, we searched for objects among the 95 NEAs and MCAs included in this study that have a negligible probability of having a close encounter with any planet. To quantify this, we calculated the probability $P(R, t)$ that an individual object in our sample had an encounter with $r < R = 20 R_{\text{pl}}$ in the past $t = 0.5$ My (Fig. 3). We found that nineteen out of twenty S/Sq asteroids listed in B10 as having MOID³ outside the lunar distance also have $P(20, 0.5) < 5\%$; only 54690 2001EB has $P(20, 0.5) = 10\%$ of having encounter with Mars.

²<http://newton.dm.unipi.it/neodyS/>

³The Minimum Orbital Intersection Distance or MOID is defined in Bonanno (2000). It is a useful indication of whether or not two objects can collide and is frequently used to identify the potentially hazardous asteroids. The information carried in MOID, however, does not indicate whether such a collision (or close encounter) is likely or not; that depends on the exact location of the two objects in their orbits. Using MOID, B10 divided objects into those with MOID corresponding to Earth encounters smaller than the lunar distance and those with MOID larger than this distance.

What is slightly more puzzling is that three asteroids with B10’s MOID values in the lunar distance also have $P(20, 0.5) < 5\%$. One of these is classified as S (719 Albert), and two are Qs (162058 1997AE12 and 2008CL1). This shows that the classification of objects based on MOID is ambiguous because it does not properly take into account the actual encounter probability over a finite time interval. It is therefore incorrect to assign the B10’s result (even approximate) statistical significance, because such a calculation will depend on the subjective choice of the cutoff value. For example, the partition of Q-type objects between $P(20, 0.5) > 5\%$ and $P(20, 0.5) < 5\%$ is not statistically unusual (unless MBAs were taken into account).⁴

When only encounters to the Earth are considered, the classification of objects based on their encounter probability becomes less ambiguous (Fig. 3). This happens because the probability of Earth encounter is a step-like function with either $P(20, 0.5) > 10\%$ or $P(20, 0.5) < 1\%$, and very few objects (6 in total; 3288, 5143, 6047, 23187, 2006NM and 2001FA1) in the intermediate range. One of these six intermediate objects, 5143 Heracles, is a Q with an Earth-encounter probability $P(20, 0.5) = 9\%$. Our 20 objects with $P(20, 0.5) < 1\%$ also have large MOID for Earth encounters according to B10.

We will consider two cases in the following text. In the first case, we will assume that the main effect on surface regolith of an asteroid is driven by tidal gravity during the asteroid’s encounters to the terrestrial planets (case 1). All planets, mainly Venus and Earth, must be considered in this case. To compare our models with the data, all 95 objects with known near-IR taxonomy will be considered as one group. In the second case, we will consider encounters to the Earth only (case 2). There is a possibility (discussed in more detail in §5) that electrically charged regolith particles (e.g., by photoelectric effect; Lee 1996) can be lofted by the Lorentz force when the asteroid passes through the Earth’s magnetosphere. Since the Earth magnetosphere extends to a larger distance than where tidal gravity could be important, its effects may potentially be relevant for distant encounters. Distant encounters with Venus and Mars need not to be considered because these planets do not have important magnetic fields. In this case, we will discard 20 objects with $P(20, 0.5) < 1\%$ for Earth

⁴So far there is not known any Q-type object among distant MCAs with $P(20, 0.5) < 1\%$ (for which we have the near-IR data). It will be interesting to see if this situation holds with new observations.

encounters (group 2 in the following) from our list and consider the remaining 75 objects only (group 1).

The SW timescale and critical encounter distance for which the tidal gravity (or Lorentz force) can be important are treated as free parameters in the following. Specifically, we determine the number of bodies in the selected sample that are expected to have at least one encounter with distance $r < r^*$ in time t , where t and r^* are free parameters. This value gives us a sense of the expected fraction of the Q-type objects in our model as a function of the SW timescale and r^* .⁵ As in B10, we use a definition of the SW timescale, t_{sw} , as the characteristic time interval during which an initially ‘fresh’ Q-type NEA affected by SW *remains* Q. This is the natural timescale that is directly constrained by the observed Q-type fraction among NEAs.

Note that our definition differs from the one used elsewhere (e.g., Jedicke et al. 2004, NJWI05, Willman et al. 2008, Vernazza et al. 2009), where the SW timescale was defined as the time interval for SW to approach/reach completion. Additional assumptions on the SW dependence on time are therefore required to compare t_{sw} , as determined here, with the SW timescales estimated elsewhere. For example, studies of asteroid families suggest that SW can partially weather a surface in ~ 1 My (Chapman et al. 2007, Mothé-Diniz and Nesvorný 2008, Vernazza et al. 2009), and then proceed towards completion during a phase that can last several Gys (Willman et al. 2008). The timescale t_{sw} that we determine in this work provides constraints on the initial stages of the SW process.

Figure 4 shows the expected fraction of Q-type objects in case 1, as defined above, as a function of $t_{\text{sw}} \leq 1$ My and r^* (see §4 for $t_{\text{sw}} > 1$ My). We find that $<1\%$ of group 2 objects have planetary encounter with $r < r^* = 10 R_{\text{pl}}$ in $t = 0.5$ My. This fraction increases to nearly 3% for $t = 1$ My. Since there are only 20 objects in group 2, it is therefore statistically unlikely that one (or more) object(s) in group 2 would have a recent encounter with $r < r^* = 10 R_{\text{pl}}$. This is consistent with current observations that indicate that none of these objects is a Q. Spectrophotometric observations of at least ~ 100 group-2 objects

⁵Note that both the tidal gravity and Earth’s magnetospheric effects should strongly decay with the encounter distance. It is therefore approximately correct to assume that the surface is reset if a close approach is made within r^* and otherwise unaffected. A more realistic resurfacing model would include more free parameters and would be difficult to constrain with the present data.

would be needed to test the NJWI05 model in a more stringent way.

Group-1 NEAs are those that have a large number of encounters with the terrestrial planets, mainly Venus and Earth. These two planets are equally important. For example, B10 estimated by neglecting Venus encounters that Earth encounters of group-1 NEAs with $r^* = 16 R_{\text{Earth}}$ are needed, if $t_{\text{sw}} = 0.5$ My, to explain the observed fraction of Q types (28%, see below). Here we repeat this calculation and find $r^* = 17 R_{\text{Earth}}$ (Fig. 5), a slightly larger value than the B10 estimate but in a reasonable agreement with it (the difference can be explained by our larger statistics). Now, including Venus encounters but neglecting those to the Earth we find that the Venus encounters with $r^* = 19 R_{\text{Venus}}$ would be required. When both the encounters to Venus and Earth are considered, however, the required encounter distance drops to $r^* = 10 R_{\text{pl}}$ (Fig. 4a). This casts doubt on the claims in B10, where it was suggested that the Earth’s tidal gravity can reset the NEA surface during encounters at $16 R_{\text{Earth}}$.

The observed fraction of Q-type NEAs can be used to constrain parameters r^* and t_{sw} (Fig. 6). This fraction is $20/95 = 0.21$ when all objects are considered (case 1 as defined above) and $20/75 = 0.28$ when only objects in group 1 are considered (case 2). In either case, the best-fit solutions are located along a hyperbola-shaped region in (r^*, t_{sw}) space. Since planetary tides during encounters with $r > r^* = 20 R_{\text{pl}}$ should be negligible, we find that $t_{\text{sw}} > 0.1$ My. This result holds unless the Earth’s magnetospheric effects are important at $r > 35 R_{\text{Earth}}$ (Fig. 5), which is unlikely.

We find that $r^* \approx 8\text{-}12 R_{\text{pl}}$ for $t_{\text{sw}} = 0.5$ My. This r^* value is probably too large compared to the expectations from the simulations of tidal effects during planetary encounters (Richardson et al. 1998, Walsh and Richardson 2008). These simulations show that the large-scale effects of tidal gravity should be minimal beyond $\sim 6 R_{\text{pl}}$ even in the most favorable case of fast ‘prograde’ rotation of the small object. Here, the prograde rotation is defined with respect to the encounter trajectory. We thus believe that $t_{\text{sw}} \sim 1$ My can probably better fit the available constraints (from NEAs and Chapman et al. 2007, Mothé-Diniz and Nesvorný 2008, Vernazza et al. 2009) because this slightly longer timescale leads to $r^* \approx 5\text{-}7 R_{\text{pl}}$. Note that these r^* values are plausible because the optically-active thin surface layer may be vulnerable to even tiniest tidal perturbations that were not considered in the simulations of Richardson et al. (1998), and Walsh and Richardson (2008). Values

$t_{\text{sw}} > 1$ My are also plausible (based on the NEA constraint only) but we are not able to deal with these longer timescales with the method described in this section.

4. NEA Model

The method described in the previous section is only approximate because it is difficult, even in the statistical sense, to reconstruct the history of past planetary encounters by numerical integrations of present orbits into the past. It is even more problematic to try to extend these numerical integrations beyond 1 My, to times comparable with the average orbital lifetime of NEAs (≈ 5 My; Bottke et al. 2002). This is because the statistical results obtained from these integrations cannot be used to retrace the real orbital evolution of individual objects from their source locations in the main belt to NEA space. Consequently, the encounter statistic obtained from such integrations would be incorrect. A different method needs to be used to circumvent this problem (and check on the results obtained in the previous section).

We used the method developed in Bottke et al. (2002; hereafter B02). B02 constructed the NEA model by tracking orbits originating from various locations in the main belt, such as the ν_6 and 3:1 resonances, and the population known as the Intermediate source Mars Crossers (IMCs for short). IMCs have marginally unstable orbits that are leaking from more stable locations in the inner main belt but have not yet reached Mars-crossing space (Migliorini et al. 1998, Morbidelli and Nesvorný 1999). By calibrating the orbital distribution obtained in the model to that of known NEAs, B02 was able to set constraints on the contribution of each source to the NEA population as a function of absolute magnitude H . Apparently, the three most important sources are the ν_6 resonance, 3:1 resonance and IMCs, which contribute by 37%, 20% and 27%, respectively, for $H < 18$. [The outer main belt resonances and Jupiter-family comets provide the remaining 16%.]

We conducted numerical simulations similar to those reported in B02 only this time focusing on the statistics of close encounters of NEAs with the terrestrial planets. Specifically, we tracked orbits of ~ 1000 test particles (per source) as they evolve from their source regions into planet-crossing space. These integrations included seven planets (Venus to Neptune). Thermal effects on orbits (such as the Yarkovsky effect) were neglected because NEA dynam-

ics is mainly controlled by planetary encounters and powerful resonances. We used a variant of the Wisdom-Holman map (Wisdom and Holman 1991) known as `Swift_rmvs3` (Levison and Duncan 1994). We modified the Swift integrator so that it records all encounters of model NEAs with planets up to a distance of $20 R_{\text{pl}}$.

These data were used in a statistical model that follows the orbital evolution of each object and estimates its spectral index at any given moment. We define the spectral index, I_s , as 0 for a fresh Q-type object and 1 for a fully space weathered S type object. The intermediate values $1/3 < I_s < 2/3$ are used to represent the Sq-type asteroids. The model has two parameters: r^* and t_{sw} . Each object is assumed to be initially fully space weathered with $I_s = 1$. If an encounter with $r < r^*$ occurs, we set $I_s = 0$ at the corresponding time, and let a simple SW algorithm increase I_s . Therefore, assuming that no additional encounters with $r < r^*$ happen in the interim interval, $I_s = 1/3$ after t_{sw} has elapsed. Parameter t_{sw} thus represents the timescale during which an initially fresh Q-type asteroids remains Q. This definition is consistent with the one used in the previous section.

Note that our algorithm is only a simple representation of the SW process that, in reality, must be more complicated. For example, Jedicke et al. (2004) and Willman et al. (2008) assumed that the spectral slope has an exponential dependence on time (as if SW were produced by constant SW agent), and defined the SW timescale as the characteristic exponential time scale, τ , of this dependence. The relationship between our t_{sw} and their τ is $t_{\text{sw}} = -\ln(2/3)\tau \approx 0.4\tau$, where $\tau \sim 1$ Gy in Willman et al. (2008). This suggests that t_{sw} could be very long. On the other hand, Vernazza et al. (2009) invoked a two-step process with the fast initial stage, perhaps due to ion sputtering, and slower later stage, as in Willman et al. (2008). These two-step process would indicate that $t_{\text{sw}} \lesssim 1$ My (Chapman et al. 2007, Mothé-Diniz and Nesvorný 2008).

We run our code over all test orbits and record I_s as a function of a , e and i . The expected fraction of Q-type NEAs in a given orbital bin, $f_Q(a, e, i)$, is then estimated as $f_Q = N(I_s < 1/3)/N$, where N and $N(I_s < 1/3)$ are the total number of recorded cases and the number of cases with $I_s < 1/3$, respectively. The contribution of particles starting in different sources is weighted by the relative importance of each source according to B02. Fractions $f_Q(a, e, i)$ obtained in this NEA model with different r^* and t_{sw} are then compared with the observed fraction of Q-type NEAs. This comparison helps us to set constraints on

the SW timescale and critical encounter distance.

With only 20 known Q-type objects the current spectrophotometric catalog of NEAs is largely incomplete and probably biased by the observer’s selection criteria that are difficult to characterize. We do not make any attempt to compensate for the observational bias. To compare our model with the sparse data, we find that the best strategy is to divide the orbital region into large bins in the perihelion and aphelion distance, and inclination. This is useful because large bins allow for better statistics. It is also better to use q , rather than a or e , because the orbital distribution of Q-type NEAs has a sharp edge at $q = 1$ AU with no Q-types known with $q > 1.1$ AU (Fig. 1).

Simulated fraction f_Q is compared with observations using the usual χ^2 statistics. Given the dependence of the statistics on the bin selection, however, we do not attempt to assign any formal confidence levels to various parameter choices. Instead, we only compare different models relatively among themselves according to their χ^2 value; models with smallest χ^2 are given priority.

Figure 7 shows the χ^2 values for models with different r^* and t_{sw} . The range of parameter values that fits observations best roughly overlaps with the region identified from backward numerical integrations in §3 (cf. Fig. 6). This gives some credibility to the method used in §3.

We find that $t_{\text{sw}} < 0.1$ My can be rejected unless $r^* > 20 R_{\text{pl}}$, in a good agreement with the results obtained in §3. Figure 7b extends these results to $t_{\text{sw}} = 35$ My. The best fits occur along a curve that indicates progressively smaller r^* values for longer t_{sw} . Eventually, the fits following this curve slightly degrade for $t_{\text{sw}} > 30$ My. Also, $r^* < 2 R_{\text{pl}}$ for $t_{\text{sw}} > 35$ My, while $r^* > 2 R_{\text{pl}}$ according to Richardson et al. (1998). These long SW timescales therefore do not appear plausible.

Fraction $f_Q(a, e, i)$ obtained in our model is shown in Figs. 8-10 for several different values of t_{sw} and r^* . Figure 8 shows f_Q for $r^* = 10 R_{\text{pl}}$ and $t_{\text{sw}} = 0.1$ My, and $r^* = 5 R_{\text{pl}}$ and $t_{\text{sw}} = 15$ My. Both these parameter choices do not fit observations well. The one with $t_{\text{sw}} = 0.1$ My produces an overall excess of Q-type objects with $f_Q > 0.5$ for $q < 1$ AU and $a < 2$ AU. The one with $t_{\text{sw}} = 15$ My shows $f_Q < 0.1$. In comparison, the surveyed NEAs have $f_Q = 0.2$ -0.3 overall. Note that the two models illustrated in Fig. 8 lay outside the

low- χ^2 region shown in Fig. 7.

Two of our models that match observations better are illustrated in Fig. 9 ($r^* = 7 R_{\text{pl}}$ and $t_{\text{sw}} = 1 \text{ My}$) and Fig. 10 ($r^* = 2.5 R_{\text{pl}}$ and $t_{\text{sw}} = 15 \text{ My}$). These models correspond to some of the lowest χ^2 values that we have obtained. Fraction f_Q increases in both these models with decreasing heliocentric distance. In Fig. 9, the model with $t_{\text{sw}} = 1 \text{ My}$ produces a concentration of Q-type objects with low orbital inclinations, while in Fig. 10 the model with $t_{\text{sw}} = 15 \text{ My}$ shows a more equal distribution of f_Q in inclination. These differences could be used to discriminate between short and long SW timescales, even without an explicit constraint on r^* , when spectroscopic observations of NEAs become more complete.

While the overall fraction of Q-type NEAs in Figs. 9 and 10 closely matches current observations, the model distribution of Qs in orbital space differs in one important aspect from the one shown in Fig. 1. It shows a large gradient with semimajor axis with Q-type objects being rare beyond 1.5 AU. Conversely, the observed distribution is flat in a with a significant fraction of Qs having $a > 1.5 \text{ AU}$. Some unspecified observational selection effect may be responsible for this discrepancy. Alternatively, this problem may indicate that the SW timescale is a function of a (Marchi et al. 2006).

If, for example, the solar wind sputtering controls t_{sw} we would expect that $t_{\text{sw}} \propto 2\pi / \int h^{-2} = 2q^2(1+e)^2/(2+e^2)$, where h is the heliocentric distance and the integral was taken over orbit.

Figure 11 shows $f_Q(a, e, i)$ for $r^* = 7 R_{\text{pl}}$ and $t_{\text{sw}} = 1 \text{ My} \times 2q^2(1+e)^2/(2+e^2)$ with a in AU. As expected, the model distribution is flatter in a with $f_Q \sim 0.2$ for $a > 1.5 \text{ AU}$ and $0.5 < q < 1 \text{ AU}$. This fits observations in this orbital range rather nicely (better than our nominal model with fixed t_{sw}). Note, however, that it fails to explain 5 Q-type NEAs with $a \lesssim 1 \text{ AU}$ and $q < 0.5 \text{ AU}$ that represent $\sim 50\%$ of surveyed chondritic NEAs in this region (see §5 for a discussion). The implication of this model is that $t_{\text{sw}} > 1 \text{ My}$ in the main asteroid belt. In §5, we discuss how this fits the independent constraints obtained on t_{sw} from studies of asteroid families.

5. Discussion

Several tidal effects may disturb the surface of a NEA during a distant planetary encounter.⁶ For example: (1) The interior structure of a rubble-pile asteroid may find a new equilibrium by re-arranging its components. This motion can produce landslides, degrade craters, ballistically displace surface material, or even remove the original layers from the asteroid. (2) Tidal stresses applied to a fractured interior may produce seismic shakes similar to, or perhaps more effective than, those generated by impacts. Consequently, surface morphology may be modified. (3) The tidal torque may spin up an asteroid. In surface segments where the centrifugal force exceeds gravity, regolith layers will be removed by carrying away the excess angular momentum. More subtle changes can occur in other surface parts of a spun-up asteroid. (4) If the tidal force becomes comparable to the object’s gravity during encounter, an asteroid with large enough internal strength and a strengthless regolith may lose its regolith layer.

These effects and their dependence on the encounter distance and speed are poorly understood. Some insights into this problem can be obtained from Richardson et al. (1998), where the authors performed numerical simulations of the effects of tidal gravity on a small asteroid with strengthless (rubble-pile) interior. In the most favorable case (slow encounter speed, fast prograde rotation), they found that significant mass shedding can occur up to $\approx 5 R_{\text{pl}}$. This sets a soft constraint on r^* . On one hand, r^* can be larger than $5 R_{\text{pl}}$ because the optically-active thin surface layer may be vulnerable to even tiniest perturbations that were not considered in the Richardson et al. model. On the other hand, when averaging over all encounter geometries and plausible asteroid spin states, the mean r^* can become lower than $5 R_{\text{pl}}$. Thus, for the lack of additional constraints on r^* , we will tentatively assume below, as a guideline for discussion, that $r^* \sim 5 R_{\text{pl}}$.

If we set $r^* = 5 R_{\text{pl}}$ our results described in §3 and §4 imply that $t_{\text{sw}} \sim 1$ My. At first sight, this SW timescale seems to be comparable to that obtained from comparative studies of asteroid families in the main belt and OC meteorites in the RELAB database (NJWI05, Vernazza et al. 2009). For example, Vernazza et al. (2009) proposed that the SW timescale

⁶We only discuss distant encounters here. It is clear that the SL9-like tidal disruption, binary formation events, or events with significant mass shedding will erase any pre-existing surface features.

is $\lesssim 1$ My. Their result hinges on observations of two largest members of the Datura family that formed by a catastrophic breakup ≈ 0.5 My ago (Nesvorný et al. 2006, Vokrouhlický et al. 2009). These two objects, 1270 Datura and 90265 2003CL5, appear to be significantly (but not completely) space weathered (Mothé-Diniz and Nesvorný 2008), which implies that the SW timescale should be comparable to or shorter than the Datura family’s age. This poses a problem because $t_{\text{sw}} \lesssim 0.5$ My does not fit the NEA constraint (unless $r^* > 5 R_{\text{pl}}$). Below we discuss possible solutions to this problem.

Observations of 2001 WY35, one of the smallest known members of the Datura family (absolute magnitude $H = 17$), indicate that this object is not space weathered at all (Mothé-Diniz and Nesvorný 2008). If these observations were correct, they would indicate that (at least some) km-sized asteroids may weather on timescales significantly longer than ≈ 0.5 My. For example, small km-sized fragments ejected from asteroid breakup events may not retain/accumulate sufficient regolith layer on their surface in the immediate aftermath of the collision. The SW effects may be delayed for such objects until a particulate (SW-sensitive) surface layer develops on their surface, for example, by subsequent impact shattering of the exposed rock. Thus, the regolith formation and ‘gardening’ can be an important part of the problem (Jedicke et al. 2004, Willman et al. 2008).

We should not forget that the two constraints on the SW timescale discussed here come from studies of two distinct population of objects that are affected by different physical processes. The asteroids in the main-belt families are born by violent collisions and spend most of their lifetime beyond 2 AU. The NEAs, on the other hand, are exposed to more extreme solar-wind and temperature environment. They are olivine-rich and may therefore be more susceptible to SW effects than an average MBA (Sasaki et al. 2001, Marchi et al. 2005). While large impacts on NEAs should be rare, bombardment of their surface by $D \sim 100 \mu\text{m}$ particles should be more intense than on MBAs due to the larger number density of micrometeoroids at < 2 AU (Grün et al. 1985). Also, distant planetary encounters of NEAs should produce more gentle effects than catastrophic collisions of MBAs, thus giving the initial surface different attributes. In summary, the *proper* SW timescale that measures the progression of SW under ideal conditions (e.g., in absence of regolith gardening) may be substantially shorter than the *apparent* SW timescale that arises from combination of different effects, and these effects most likely operate on different timescales in the NEA and

MBA environments.

Another interesting possibility is related to the effects of the Earth magnetosphere on loose particulate material on a small asteroid’s surface. The Earth magnetosphere extends to $\approx 12 R_{\text{Earth}}$ in the direction toward the Sun, $\approx 15 R_{\text{Earth}}$ in apex and antapex directions, and $\approx 25 R_{\text{Earth}}$ the anti-helion direction. The tail region stretches well past $200 R_{\text{Earth}}$, and the way it ends is not well-known. The magnetic field ranges from 30-60 μT at the Earth’s surface and falls roughly as $1/r^3$ with distance r toward the edge of the magnetosphere. Thus, if a 100-m-sized NEA passes at distance $10 R_{\text{Earth}}$, a 10- μm surface dust grain subject to the Lorentz force would levitate if previously charged to $> 10^8 e$. Such charge is plausible for an asteroid surface of sufficiently high electrical resistivity. It is not clear, however, whether the Lorentz force effect can be more significant than the electrostatic levitation (Lee 1996) and/or van der Waals forces (Scheeres and Hartzell 2010).

While speculative, the effects of Earth magnetosphere could possibly allow for larger r^* values than those expected for tidal gravity. This could perhaps help to resolve some of the discrepancy between different measurements of the SW timescale discussed above. For example, with $r^* = 20 R_{\text{Earth}}$, Fig. 5 would imply that $t_{\text{sw}} \approx 0.25 \text{ My}$.

The orbits of Q-type NEAs in Fig. 1 hint on bimodal distribution with a group of 7 objects with $a \lesssim 1 \text{ AU}$ and largely spread inclination values, and 12 objects with $a \gtrsim 1.5 \text{ AU}$ and $i \lesssim 10^\circ$. Using planetary encounters as the main agent that resets the SW clock, we were not able to fit both groups simultaneously. We found that the model with fixed t_{sw} can match the low- a group but it fails to fit the observed fraction of Qs with $a > 1.5 \text{ AU}$ (e.g., Fig. 9). On the other hand, the model with $t_{\text{sw}} \propto q^2$ matches the high- a group (Fig. 11) but it fails to produce the observed large fraction of Qs with $a \lesssim 1 \text{ AU}$ and $q < 0.5 \text{ AU}$.

This is puzzling. The problem may be related to biases in the current sparse spectrophotometric data. Alternatively, we may be missing some important physical effect in the model. For example, a small irregular object can be spun up by a radiation effect known as YORP and shed mass (e.g., Walsh et al. 2009; see Bottke et al. 2006 for a recent review of YORP). This could lead to a partial or global removal of the space weathered material and exposure of fresh material on the surface. This effect can therefore be important. Unfortunately, the timescale on which the surface of a typical NEA can be reset by YORP is

poorly understood.

Kaasalainen et al. (2007) determined that 1862 Apollo ($a = 1.47$ AU, $D = 1.4$ km) is spun up by YORP on a characteristic timescale $t_{\text{YORP}} = \omega/(d\omega/dt) \sim 2.6$ My, where ω is the spin rate. Starting from its current 3-hour spin period, 1862 Apollo is thus expected to be spun up to a ~ 2 -hour period (and start shedding mass) in ~ 2 My. This timescale is probably at least slightly longer than the one on which the surface of 1862 Apollo should be reset by planetary encounters indicating that the YORP effect can be ignored for 1862 Apollo.

Since $t_{\text{YORP}} \propto D^2 a^2 \sqrt{1-e^2}$ (e.g., Nesvorný et al. 2007), however, the YORP effect can become more important than planetary encounters for small NEAs that orbit closer to the Sun than 1862 Apollo. For example, a sub-km NEA with $a < 1$ AU can have t_{YORP} several times shorter than 1862 Apollo. We therefore speculate that the YORP effect can contribute to the observed excess of Q-type NEAs in these low- a orbits. A detailed analysis of this problem goes beyond the scope of this paper.

6. Summary

The main results obtained in this work can be summarized as follows:

1) The NJWI05 model (§2) is consistent with the current spectroscopic observations of NEAs. The effect of planetary encounters can therefore explain the tendency towards seeing the fresh OC-like material among NEAs. The fraction of Q-type asteroids in the main belt should be small because the processes that affect MBAs (e.g., collisions) lack the efficiency of planetary encounters.

2) From modeling the spectral properties of NEAs we found that the SW timescale is longer than ~ 0.1 My and shorter than ~ 10 My. It is most plausible that $t_{\text{sw}} \sim 1$ My and $r^* \sim 5 R_{\text{pl}}$. This result is in a broad agreement with t_{sw} estimated from studies of asteroid families and our current understanding of the effects of tidal gravity.

3) We found that $t_{\text{sw}} \propto q^2$, expected if the solar wind sputtering controls t_{sw} , provides a better fit to the orbital distribution of Q-type NEAs than models with fixed t_{sw} . If $t_{\text{sw}} \propto q^2$,

however, our simple model fails to explain the excess of Q-type NEAs with low- a orbits. We speculate that this population could be susceptible to the YORP effect.

4) Tidal encounters of NEAs with Venus and Earth are important, but those with Mars (and Mercury) are rare. This is mainly due to the fact that Mars is a much smaller planet than Venus and Earth and has a relatively large orbit. From the statistics of Mars encounters we estimate that a small fraction of MCAs could be Qs ($\lesssim 1\%$). This fraction should be above the main belt average. A large observational sample will be needed to test this prediction.

5) The effects of the Earth’s magnetosphere can be more important than tidal gravity for distant Earth encounters. These distant encounter effects are not required, however, to explain the observed fraction of Q-type NEAs, if $t_{\text{sw}} \sim 1$ My.

This work was funded by the NASA Planetary Geology and Geophysics program. The work of DV was also partially supported by the Czech Grant Agency (grant 205/08/0064) and the Research Program MSM0021620860 of the Czech Ministry of Education. We thank Bruce Hapke and Robert Jedicke for their very helpful referee reports.

REFERENCES

- Binzel, R. P., Bus, S. J., Burbine, T. H., Sunshine, J. M. 1996. Spectral Properties of Near-Earth Asteroids: Evidence for Sources of Ordinary Chondrite Meteorites. *Science* 273, 946-948.
- Binzel, R. P., Rivkin, A. S., Stuart, J. S., Harris, A. W., Bus, S. J., Burbine, T. H. 2004. Observed spectral properties of near-Earth objects: results for population distribution, source regions, and space weathering processes. *Icarus* 170, 259-294.
- Binzel, R. P., Morbidelli, A., Merouane, S., DeMeo, F. E., Birlan, M., Vernazza, P., Thomas, C. A., Rivkin, A. S., Bus, S. J., Tokunaga, A. T. 2010. Earth encounters as the origin of fresh surfaces on near-Earth asteroids. *Nature* 463, 331-334.
- Bonanno, C. 2000. An analytical approximation for the MOID and its consequences. *Astronomy and Astrophysics* 360, 411-416.

- Bottke, W. F., Melosh, H. J. 1996. Formation of asteroid satellites and doublet craters by planetary tidal forces. *Nature* 381, 51-53.
- Bottke, W. F., Morbidelli, A., Jedicke, R., Petit, J.-M., Levison, H. F., Michel, P., Metcalfe, T. S. 2002. Debaised Orbital and Absolute Magnitude Distribution of the Near-Earth Objects. *Icarus* 156, 399-433.
- Bottke, W. F., Durda, D. D., Nesvorný, D., Jedicke, R., Morbidelli, A., Vokrouhlický, D., Levison, H. 2005. The fossilized size distribution of the main asteroid belt. *Icarus* 175, 111-140.
- Bottke, W. F., Jr., Vokrouhlický, D., Rubincam, D. P., Nesvorný, D. 2006. The Yarkovsky and YORP Effects: Implications for Asteroid Dynamics. *Annual Review of Earth and Planetary Sciences* 34, 157-191.
- Bus, S. J., Binzel, R. P. 2002. Phase II of the Small Main-Belt Asteroid Spectroscopic Survey A Feature-Based Taxonomy. *Icarus* 158, 146-177.
- Chapman, C. R. 1996. S-Type Asteroids, Ordinary Chondrites, and Space Weathering: The Evidence from Galileo's Fly-bys of Gaspra and Ida. *Meteoritics and Planetary Science* 31, 699-725.
- Chapman, C. R. 2004. Space Weathering of Asteroid Surfaces. *Annual Review of Earth and Planetary Sciences* 32, 539-567.
- Chapman, C. R., Enke, B., Merline, W. J., Tamblyn, P., Nesvorný, D., Young, E. F., Olkin, C. 2007. Young Asteroid 832 Karin shows no rotational spectral variations. *Icarus* 191, 323-329.
- Clark, B. E., and 11 colleagues 2001. Space weathering on Eros: Constraints from albedo and spectral measurements of Psyche crater. *Meteoritics and Planetary Science* 36, 1617-1637.
- Clark, B. E., Helfenstein, P., Bell, J. F., Peterson, C., Veverka, J., Izenberg, N. I., Domingue, D., Wellnitz, D., McFadden, L. 2002a. NEAR Infrared Spectrometer Photometry of Asteroid 433 Eros. *Icarus* 155, 189-204.

- Clark, B. E., Hapke, B., Pieters, C., Britt, D. 2002b. Asteroid Space Weathering and Regolith Evolution. In *Asteroids III*, 585-599.
- DeMeo, F. E., Binzel, R. P., Slivan, S. M., Bus, S. J. 2009. An extension of the Bus asteroid taxonomy into the near-infrared. *Icarus* 202, 160-180.
- Gold, T. 1955. The lunar surface. *Monthly Notices of the Royal Astronomical Society* 115, 585.
- Gronchi, G. F., Milani A. 2001. Proper Elements for Earth-Crossing Asteroids. *Icarus* 152, 58-69.
- Grün, E., Zook, H. A., Fechtig, H., Giese, R. H., 1985. Collisional balance of the meteoritic complex. *Icarus* 62, 244-272.
- Hapke, B. 2001. Space weathering from Mercury to the asteroid belt. *Journal of Geophysical Research* 106, 10039-10074.
- Jedicke, R., Nesvorný, D., Whiteley, R., Ivezić, Ž., Jurić, M. 2004. An age-colour relationship for main-belt S-complex asteroids. *Nature* 429, 275-277.
- Johnson, T. V., Fanale, F. P. 1973. Optical properties of carbonaceous chondrites and their relationship to asteroids. *Journal of Geophysical Research* 78, 8507-8518.
- Kaasalainen, M., Ďurech, J., Warner, B. D., Krugly, Y. N., Gaftonyuk, N. M. 2007. Acceleration of the rotation of asteroid 1862 Apollo by radiation torques. *Nature* 446, 420-422.
- Lee, P. 1996. Dust Levitation on Asteroids. *Icarus* 124, 181-194.
- Levison, H. F., Duncan, M. J. 1994. The long-term dynamical behavior of short-period comets. *Icarus* 108, 18-36.
- Loeffler, M. J., Dukes, C. A., Baragiola, R. A. 2009. Irradiation of olivine by 4 keV He⁺: Simulation of space weathering by the solar wind. *Journal of Geophysical Research (Planets)* 114, 3003.

- Marchi, S., Brunetto, R., Magrin, S., Lazzarin, M., Gandolfi, D. 2005. Space weathering of near-Earth and main belt silicate-rich asteroids: observations and ion irradiation experiments. *Astronomy and Astrophysics* 443, 769-775.
- Marchi, S., Magrin, S., Nesvorný, D., Paolicchi, P., Lazzarin, M. 2006. A spectral slope versus perihelion distance correlation for planet-crossing asteroids. *Monthly Notices of the Royal Astronomical Society* 368, L39-L42.
- Masiero, J., Hartzell, C., Scheeres, D. J. 2009. The Effect of the Dust Size Distribution on Asteroid Polarization. *The Astronomical Journal* 138, 1557-1562.
- Migliorini, F., Michel, P., Morbidelli, A., Nesvorný, D., Zappalà, V. 1998. Origin of Multi-kilometer Earth- and Mars-Crossing Asteroids: A Quantitative Simulation. *Science* 281, 2022-2024.
- Morbidelli, A., Gladman, B. 1998. Orbital and temporal distributions of meteorites originating in the asteroid belt. *Meteoritics and Planetary Science* 33, 999-1016.
- Morbidelli, A., Nesvorný, D. 1999. Numerous Weak Resonances Drive Asteroids toward Terrestrial Planets Orbits. *Icarus* 139, 295-308.
- Morbidelli, A., Vokrouhlický, D. 2003. The Yarkovsky-driven origin of near-Earth asteroids. *Icarus* 163, 120-134.
- Mothé-Diniz, T., Nesvorný, D. 2008. Visible spectroscopy of extremely young asteroid families. *Astronomy and Astrophysics* 486, L9-L12.
- Mothé-Diniz, T., Jasmin, F. L., Carvano, J. M., Lazzaro, D., Nesvorný, D., Ramirez, A. 2009. Re-assessing the Ordinary Chondrites Paradox. *AAS/Division for Planetary Sciences Meeting Abstracts* 41, #53.02.
- Nesvorný, D., Vokrouhlický, D. 2007. Analytic Theory of the YORP Effect for Near-Spherical Objects. *The Astronomical Journal* 134, 1750.
- Nesvorný, D., Richardson, D., Walsh, K., Bottke, W. F., Chapman, C., Binzel, R. 2004. Modeling the Effect of Planetary Tides on Surface Regoliths of 433 Eros and NEOs. Proposal submitted to the NASA DDAP program.

- Nesvorný, D., Jedicke, R., Whiteley, R. J., Ivezić, Ž. 2005. Evidence for asteroid space weathering from the Sloan Digital Sky Survey. *Icarus* 173, 132-152.
- Nesvorný, D., Vokrouhlický, D., Bottke, W. F. 2006. The Breakup of a Main-Belt Asteroid 450 Thousand Years Ago. *Science* 312, 1490.
- Pieters, C. M., Taylor, L. A., Noble, S. K., Keller, L. P., Hapke, B., Morris, R. V., Allen, C. C., McKay, D. S., Wentworth, S. 2000. Space weathering on airless bodies: Resolving a mystery with lunar samples. *Meteoritics and Planetary Science* 35, 1101-1107.
- Rabinowitz, D. L. 1998. NOTE: Size and Orbit Dependent Trends in the Reflectance Colors of Earth-Approaching Asteroids. *Icarus* 134, 342-346.
- Richardson, D. C., Bottke, W. F., Love, S. G. 1998. Tidal Distortion and Disruption of Earth-Crossing Asteroids. *Icarus* 134, 47-76.
- Sasaki, S., Nakamura, K., Hamabe, Y., Kurahashi, E., Hiroi T. 2001. Production of iron nanoparticles by laser irradiation in a simulation of lunar-like space weathering. *Nature* 410, 555-557.
- Scheeres, D. J., Hartzell, C. M. 2010. The Relevance and Role of Cohesive Forces for Small Asteroids. *Lunar and Planetary Institute Science Conference Abstracts* 41, 1839.
- Vernazza, P., Binzel, R. P., Rossi, A., Fulchignoni, M., Birlan, M. 2009. Solar wind as the origin of rapid reddening of asteroid surfaces. *Nature* 458, 993-995.
- Vokrouhlický, D., and 12 colleagues 2009. Datura family: the 2009 update. *Astronomy and Astrophysics* 507, 495-504.
- Walsh, K. J., Richardson, D. C. 2008. A steady-state model of NEA binaries formed by tidal disruption of gravitational aggregates. *Icarus* 193, 553-566.
- Whiteley, R.J. 2001. A Compositional and Dynamical Survey of the Near-Earth Asteroids. PhD. Thesis. University of Hawaii.
- Willman, M., Jedicke, R., Nesvorný, D., Moskovitz, N., Ivezić, Ž., Fevig, R. 2008. Redetermination of the space weathering rate using spectra of Iannini asteroid family members. *Icarus* 195, 663-673.

Wisdom, J, Holman M., 1991. Symplectic maps for the N-body problem. *Astronomical Journal* 102, 1528-1538.

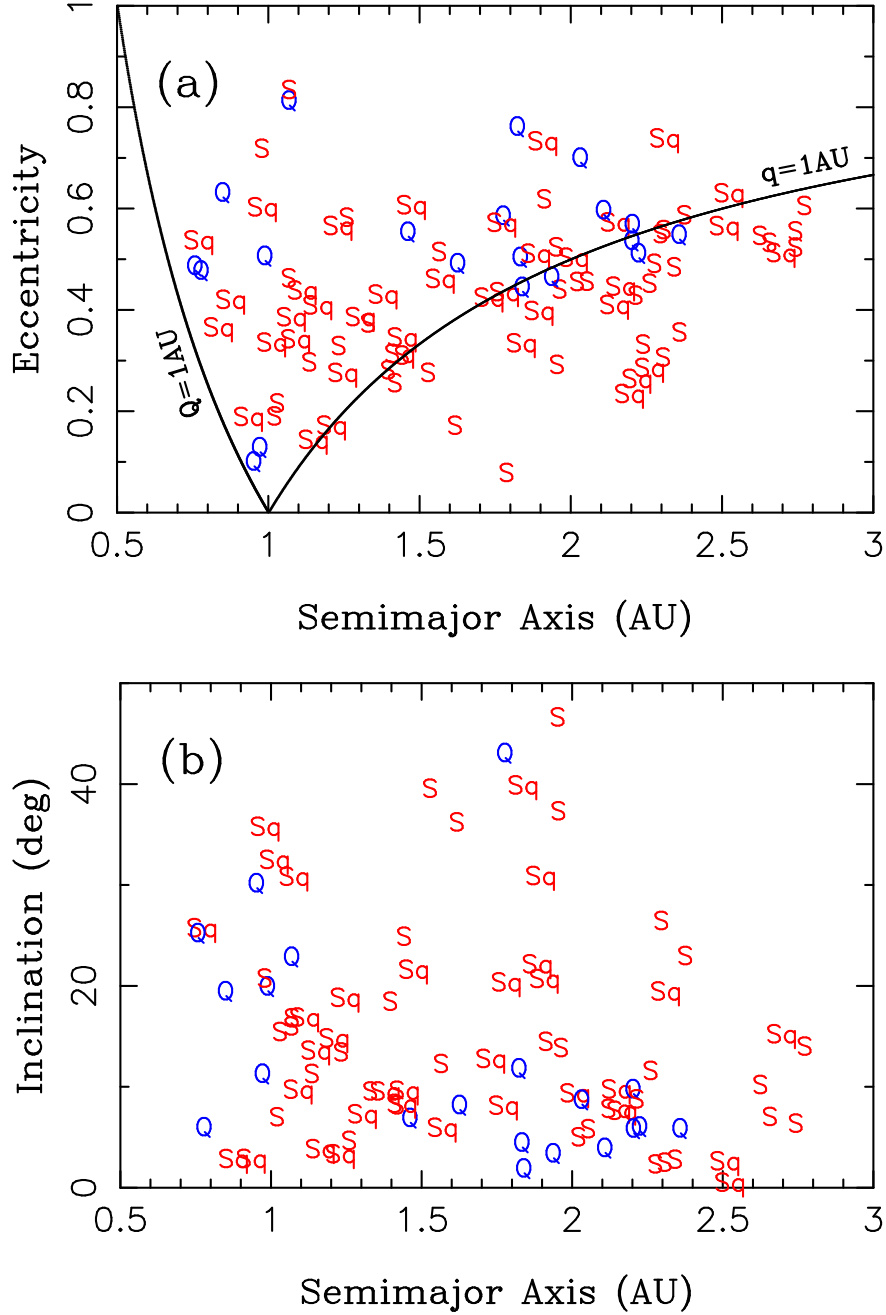


Fig. 1.— The proper orbital elements of 95 NEAs and MCAs included in this work: (a) proper semimajor axes and proper eccentricities, and (b) proper semimajor axes and proper inclinations. The proper elements of individual orbits were calculated as the arithmetic mean of minimum and maximum values given by Gronchi and Milani (2001). The symbols show the taxonomic classification of objects based on visible and near-infrared spectra (DeMeo et al. 2009). The solid lines in (a) show the proper perihelion and proper aphelion distances of 1 AU.

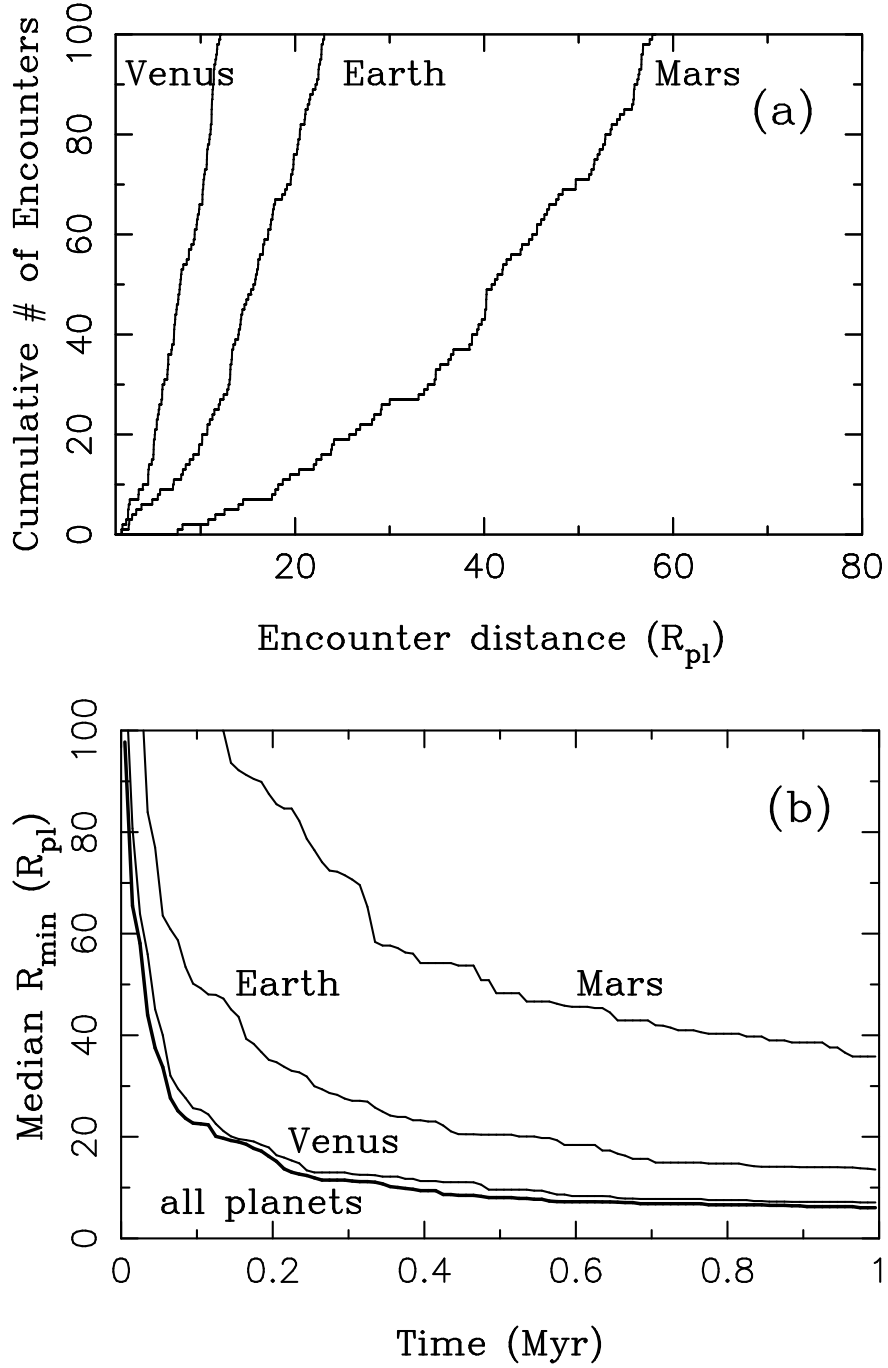


Fig. 2.— The distribution of encounters for $t = 0.5$ My (panel a) and $\bar{R}_{\text{min}}(t)$ (panel b) for asteroid 1862 Apollo. Different lines correspond to encounters with Venus, Earth and Mars. Close encounters of 1862 Apollo with Mercury are rare. This plot illustrates that the encounters with Venus are the dominant type of encounters for NEAs such as 1862 Apollo. The bold line in (b) shows $\bar{R}_{\text{min}}(t)$ when encounters to all planets are considered. In (a), a hundred of closest encounters are shown.

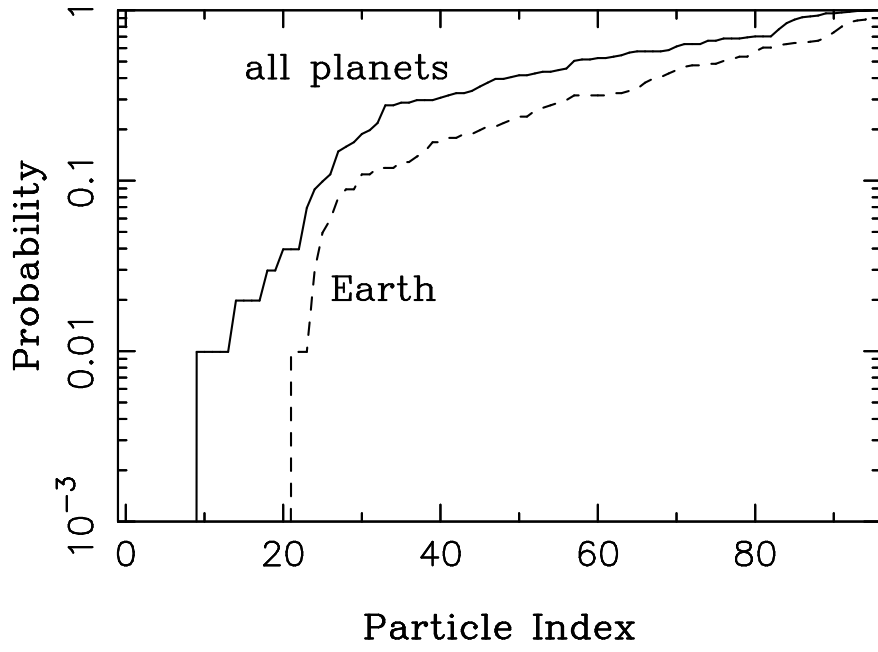


Fig. 3.— The probability of having an encounter with $r < 20 R_{\text{pl}}$ in $t = 0.5$ My. Particle index denotes individual objects that were ordered by the increasing probability value. The dashed and solid lines show the probability for encounters with the Earth and all planets, respectively.

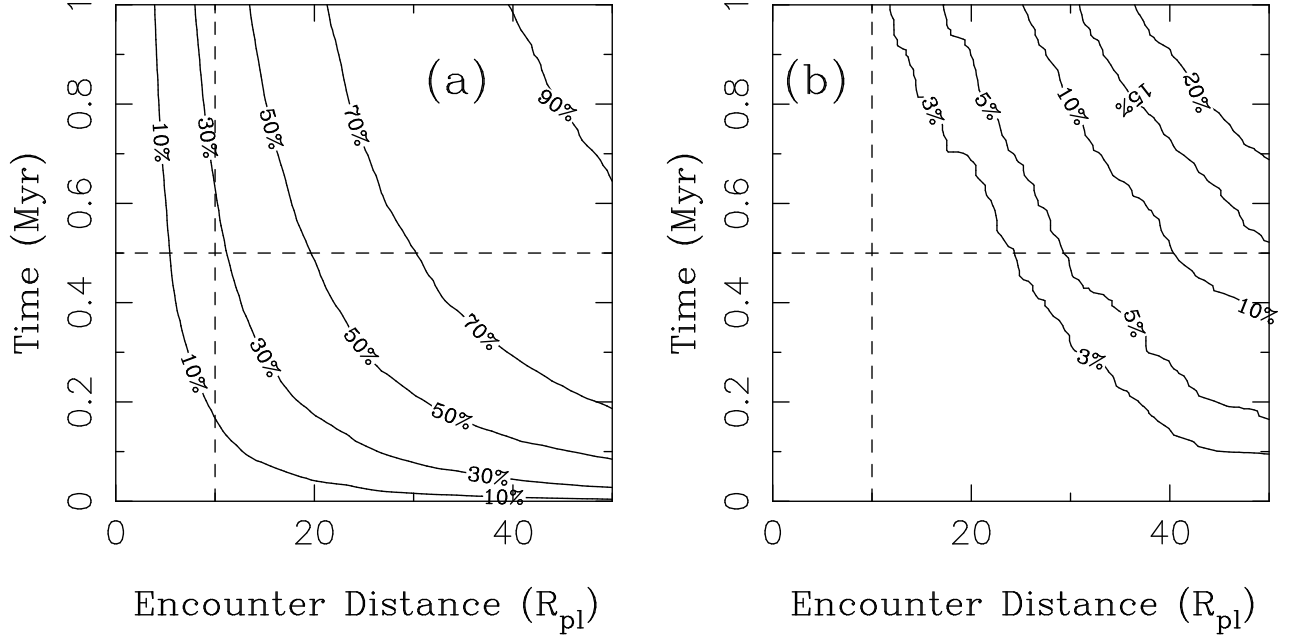


Fig. 4.— The fraction of objects having a planetary encounter with distance $r < r^*$ in time t : (a) group 1 (75 NEAs with high encounter probability); and (b) group 2 (20 NEAs and MCAs with low encounter probability). All planets are considered here. For reference, the dashed lines show $t = 0.5$ My and $r^* = 10 R_{\text{pl}}$. With $t = 0.5$ My we find that roughly 28% of objects in group 1 have a planetary encounter with $r < 10 R_{\text{pl}}$. We do not have enough resolution in the model to directly compute the fraction of group 2 objects for $t = 0.5$ My and $r^* = 10 R_{\text{pl}}$. By extrapolating the trend from larger t and r^* , we roughly estimate that this fraction is $\sim 0.5\%$.

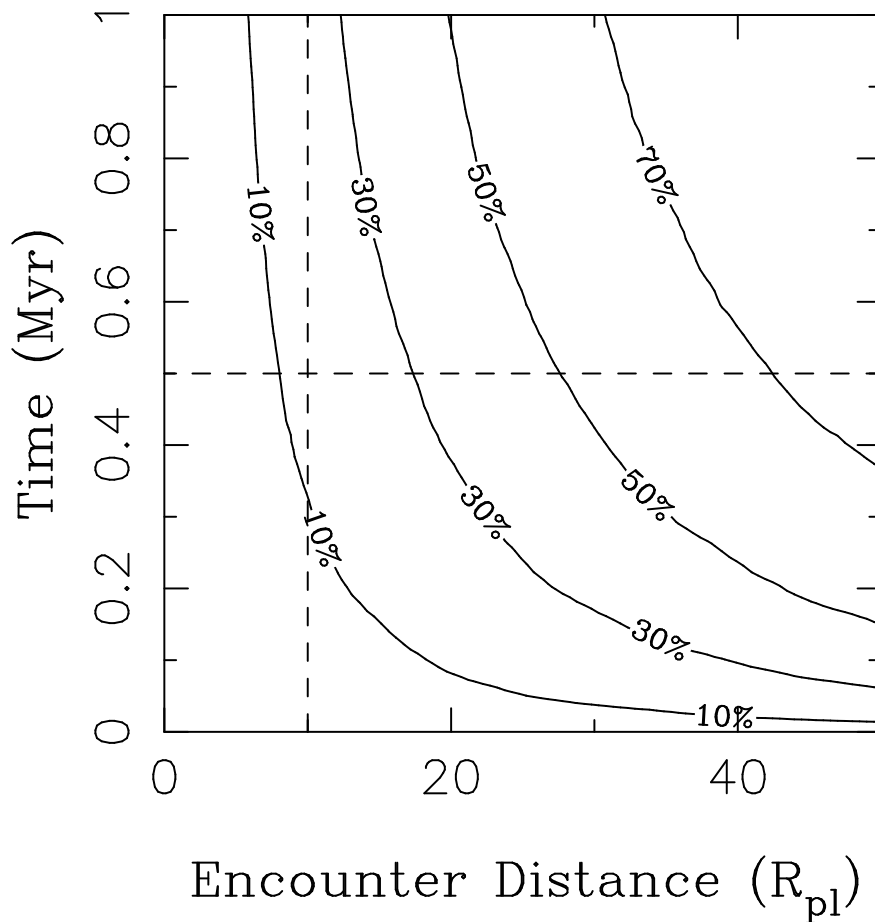


Fig. 5.— The fraction of group-1 objects having Earth encounter with distance $r < r^*$ in time t . With $t = 0.5$ My we find that roughly 28% of objects in group 1 have Earth encounter with $r < 17 R_{\text{Earth}}$. For reference, the dashed lines show $t = 0.5$ My and $r^* = 10 R_{\text{pl}}$.

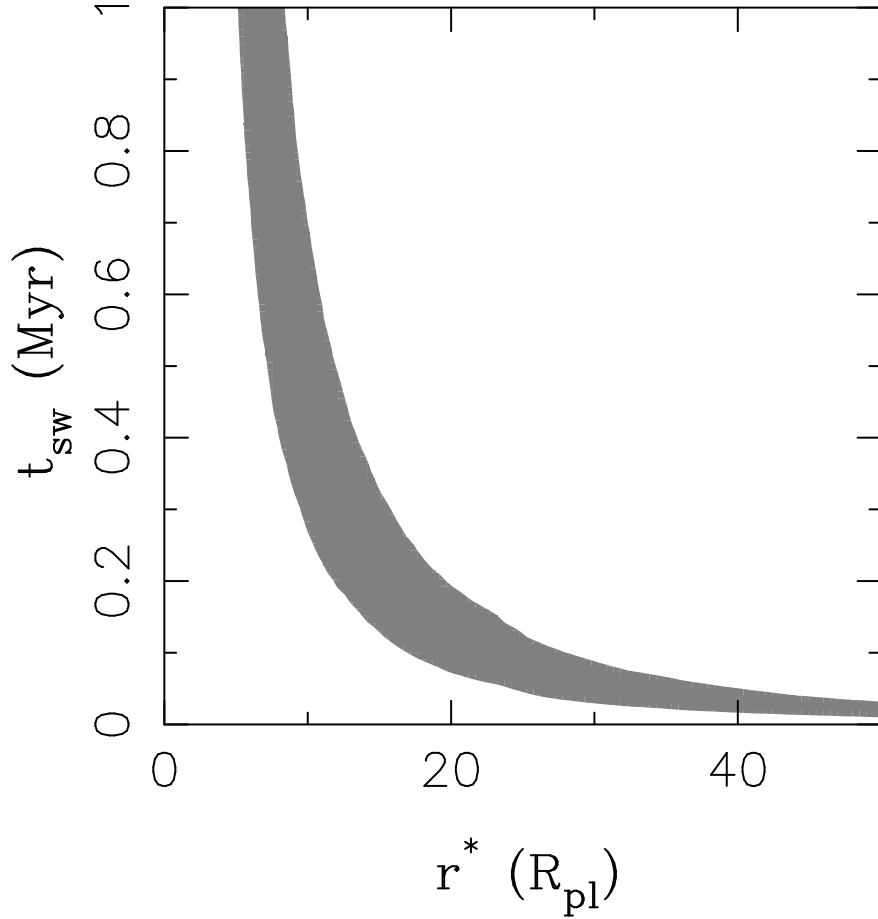


Fig. 6.— The preferred solutions according to the model described in §3. The shaded region shows the range of fractional values between 16% to 26%. All 95 selected asteroids and encounters to all planets were considered here (case 1). The range of preferred solutions remains nearly the same when only group-1 NEAs are considered. This is because their slightly larger overall encounter probability is compensated by a larger fraction of Q-type NEAs observed in that group.

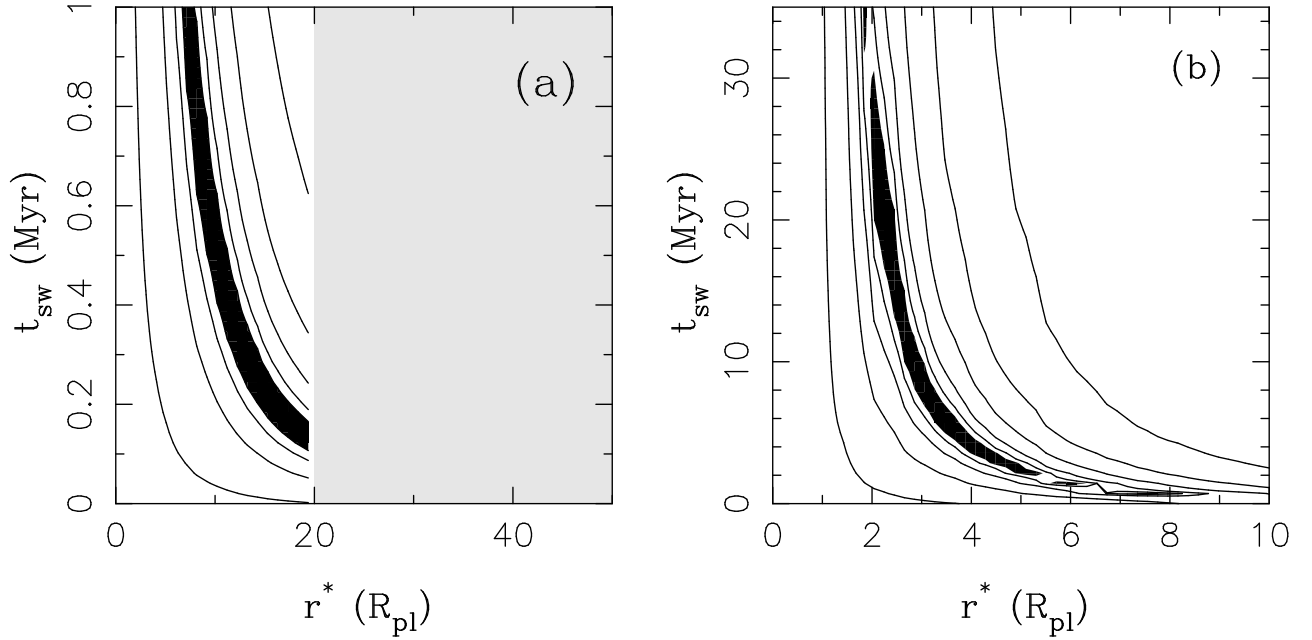


Fig. 7.— The χ^2 contours in (r^*, t_{sw}) plane. We used the NEA model to estimate $f_Q(a, e, i)$ for: (a) $t_{\text{sw}} < 1$ My, and (b) $t_{\text{sw}} < 35$ My. The distribution was compared to observations. The black-shaded area shows our best-fit parameter values. Each pair of lines that envelops the shaded area shows χ^2 contours that are spaced by a multiplication factor of 3. We have not followed encounters with $r > 20 R_{\text{pl}}$ in the NEA model described in §4. The range on X and Y axes in (a) is set to facilitate a direct comparison with Fig. 6.

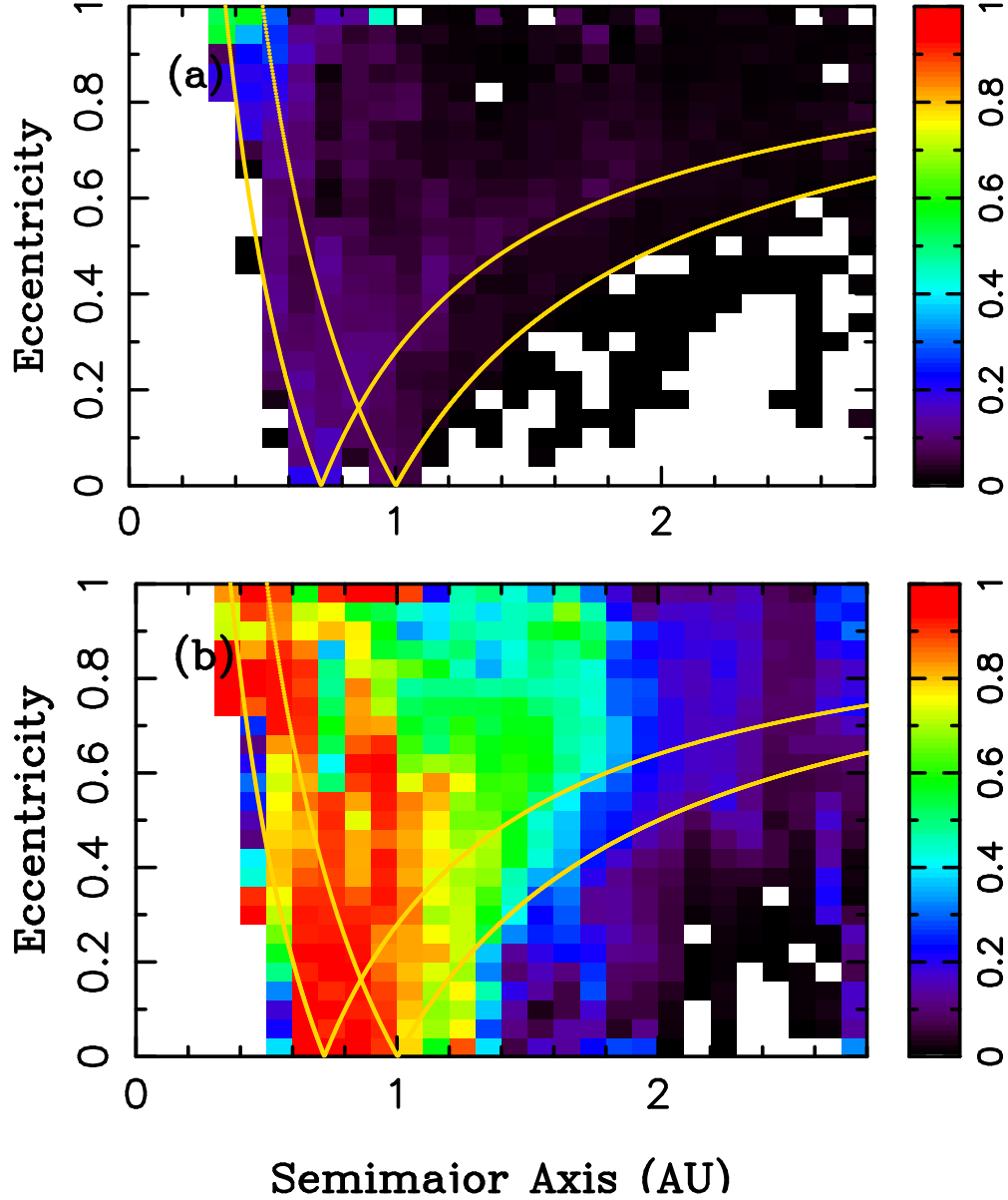


Fig. 8.— The orbital distribution of Q-type objects expected from the NEA model with: (a) $r^* = 10 R_{\text{pl}}$ and $t_{\text{sw}} = 0.1 \text{ My}$, and (b) $r^* = 5 R_{\text{pl}}$ and $t_{\text{sw}} = 15 \text{ My}$. The color scheme shows the expected number of Q-type objects in each bin as a fraction, f_Q , of the total number of objects in that bin. The red region shows orbits with the largest model concentrations of Q-type NEAs. Both these model parameters are clearly implausible because f_Q is too small in (a) and too large in (b).

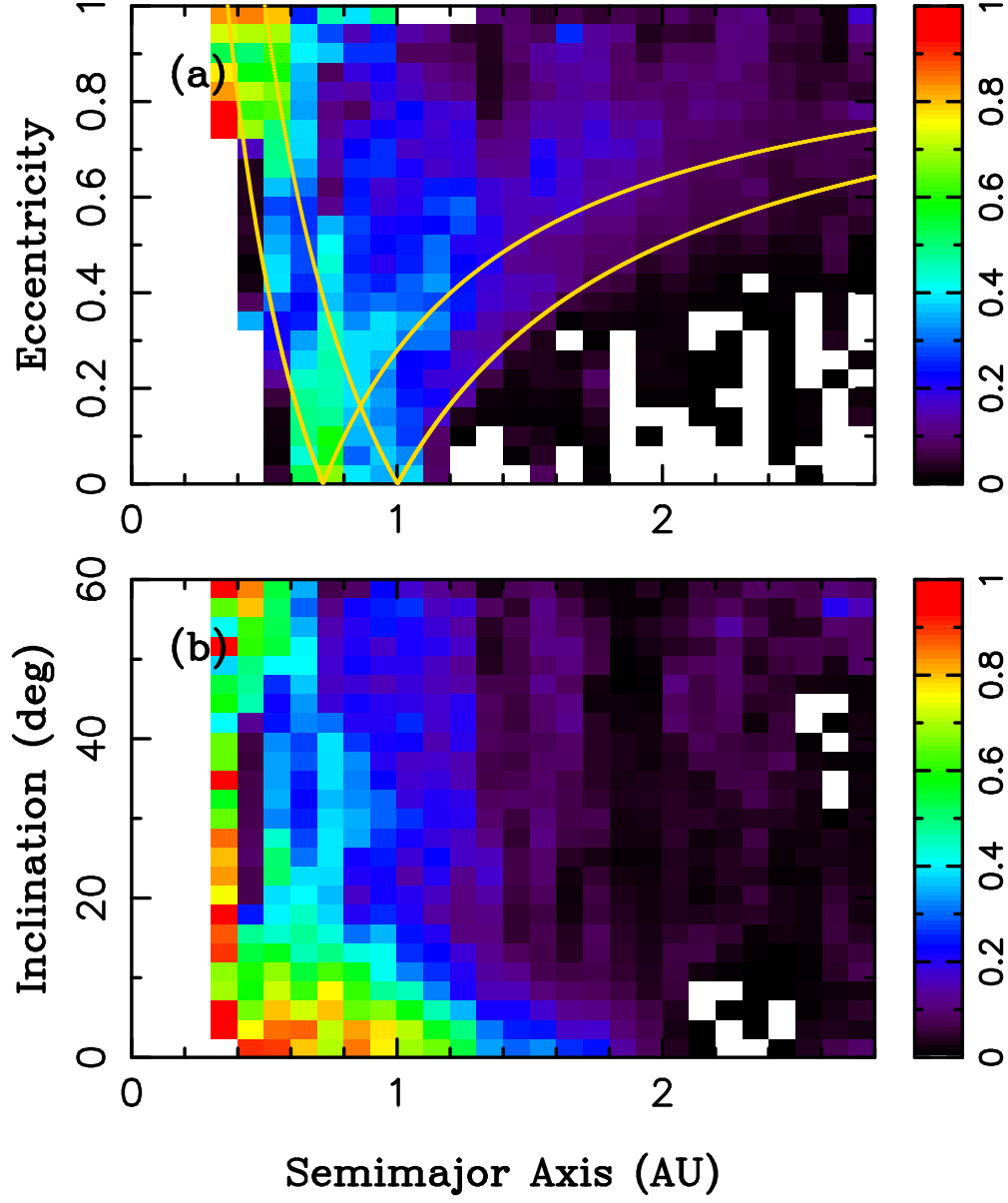


Fig. 9.— The orbital distribution of Q-type objects expected from the NEA model with $r^* = 7 R_{\text{pl}}$ and $t_{\text{sw}} = 1 \text{ My}$. The color scheme shows the number of Q-type objects in each bin as a fraction of the total number of objects in that bin.

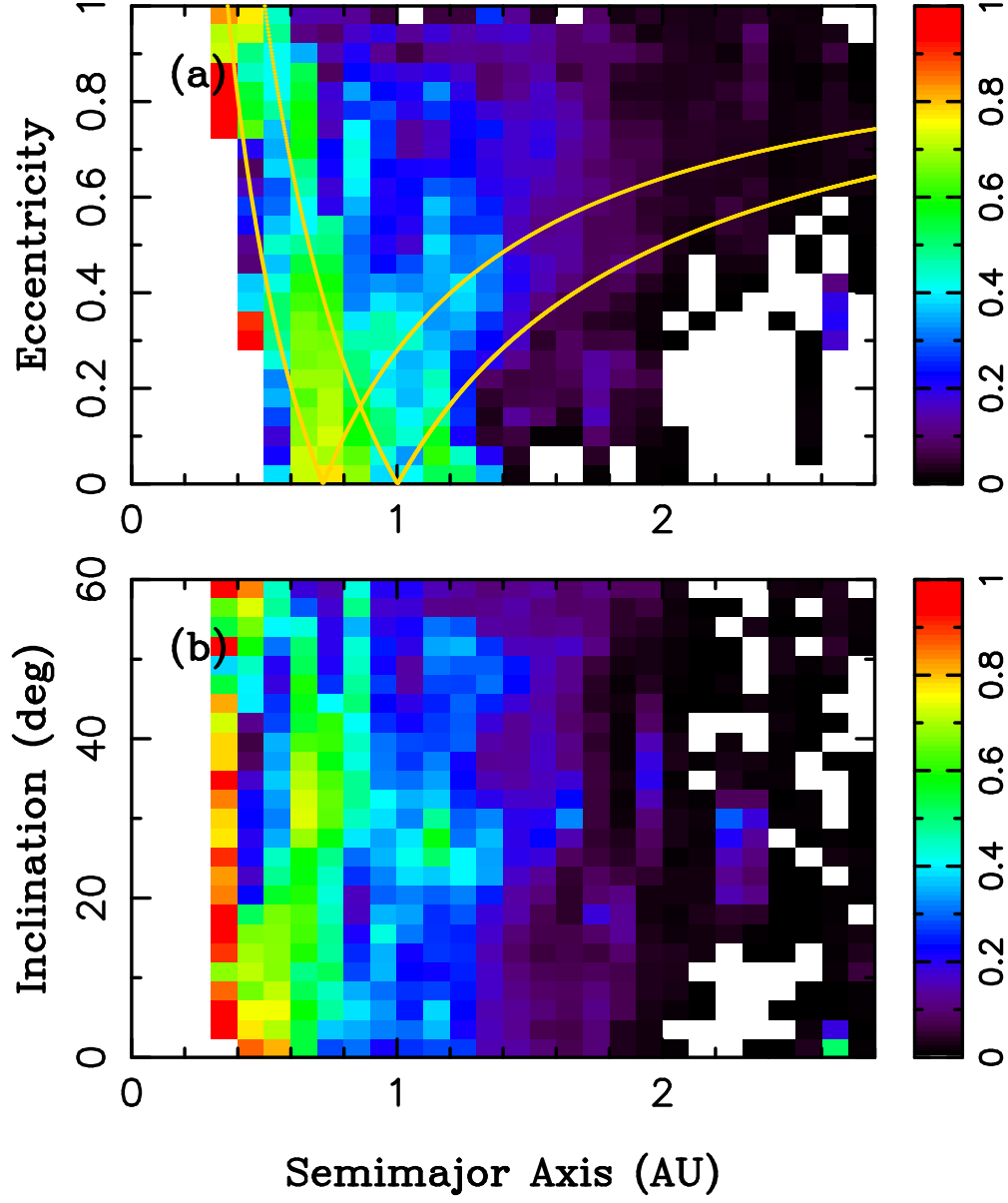


Fig. 10.— The orbital distribution of Q-type objects expected from the NEA model with $r^* = 2.5 R_{\text{pl}}$ and $t_{\text{sw}} = 15$ My. The color scheme shows the number of Q-type objects in each bin as a fraction of the total number of objects in that bin.

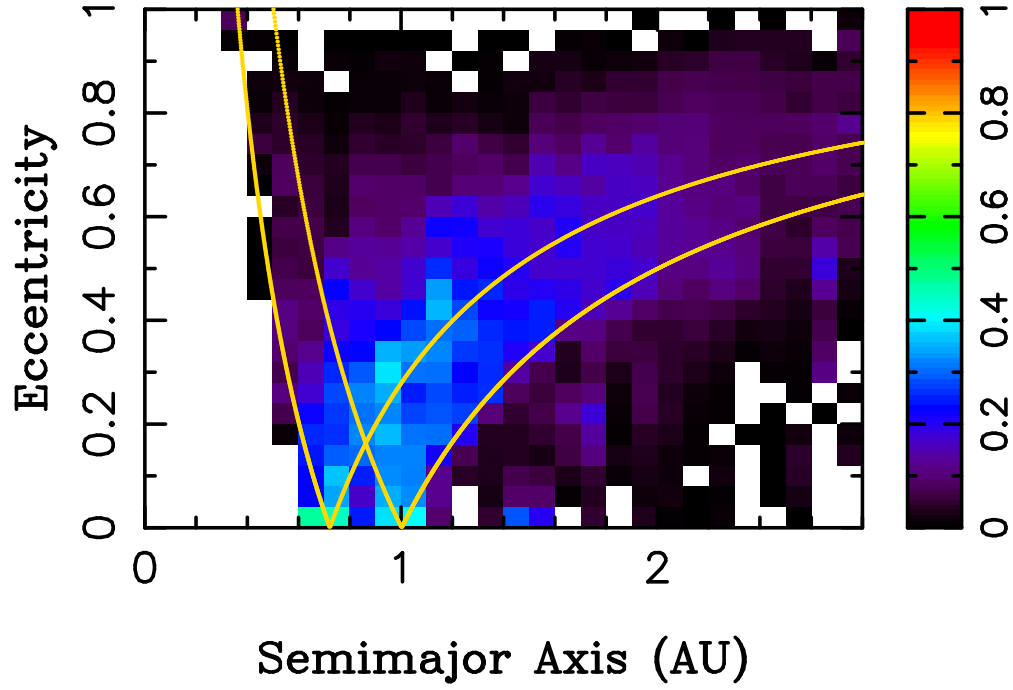


Fig. 11.— The orbital distribution of Q-type objects expected from our NEA model with $r^* = 5 R_{\text{pl}}$ and t_{sw} that depends on heliocentric distance. Here we fixed $t_{\text{sw}} = 1$ My for a circular orbit with $a = 1$ AU and increased t_{sw} roughly as q^2 with perihelion distance. The (a, i) projection, not shown here, is very similar to Fig. 9b.